ChemistrySelect

Chemistry Europe
European Chemical Societies Publishing

LATEST ISSUE >
Volume 7, Issue 5
February 4, 2022

Editor: Anne Deveson; Deputy Editor: Jonathan Faiz; Editorial Board Chairs: Dennis Hetterscheid, Hélène Lebel, An-Hui Lu
Impact factor: 2.109
2020 Journal Citation Reports (Clarivate Analytics): 116/179 (Chemistry, Multidisciplinary)
Online ISSN: 2365-6549

About

ChemistrySelect publishes good quality international research from all areas of chemistry. It is

ie, an association of 16 European chemical societies. Find out

Submit a Manuscript

Browse free sample issue

Energy Technology & Environmental Science

Enhanced Charge- Discharge Behaviour of $MnFe_2O_4$ laden Composite Cathode for Lithium-Sulfur Batteries

Deepa Elizabeth Mathew,[a, b] G. Jenita Rani,[c] D. Ponraj Jenis,[d] Sabu Thomas,[e] and A. Manuel Stephan*[a]

The Li–S battery commercialization has been hampered owing to challenging problems such as poor conductivity of elemental sulfur, volume change upon cycling, and shuttling of lithium polysulfide between the electrodes. To conquer these issues, a sensible electrode structure design is crucial. The incorporation of carbonaceous materials and metal oxides has been identified as an effective tool to foster the electrochemical properties of Li–S batteries. In this work, to confine polysulfide shuttling and to improve the conductivity of sulfur, $MnFe_2O_4$-seated rGO-sulfur composite was prepared and used as a cathode. The lithium-sulfur cell with $MnFe_2O_4$-seated rGO-sulfur composite cathode showed outstanding electrochemical performance delivering a discharge capacity of 1300 mAh g^{-1} at 0.1 C-rate on its first cycle and a stable cycling was attained at 0.5 C-rate. In the composite cathode, each component functions for a specific reason: the rGO in the composite improves the conductivity of sulfur, while added- $MnFe_2O_4$ not only confines polysulfides appreciably but also provides integrity to the cathode as evidenced by SEM analysis. The self-discharge studies showed that the Li–S cell with $MnFe_2O_4$ was capable of retaining its charge even after 90 h which has overhead the earlier reports. The Li–S system with $MnFe_2O_4$ -laden cathode material exhibited better electrochemical properties than the un-laden one.

Introduction

Lithium-sulfur battery system based on the electrochemical reaction $S_8 + 16Li^+ + 16\,e^- \leftrightarrow 8Li_2S$ has been identified as a futuristic energy storage device owing to its unique characteristics such as exceptionally high theoretical specific capacity, energy density (2600 Wh kg^{-1}), low cost, huge abundance on elemental sulfur on earth's crust and better safety.[1,2] Even though the prototype Li – S cell was invented three decades ago, the issues such as the insulating nature of elemental sulfur and shuttling of polysulfides between the electrodes impede this system from commercialization. Numerous studies have been made to conquer these challenges by engineering novel sulfur cathode structures,[3] electrolytes,[4] functionalization of separators[5] and modified binders.[6]

The sulfur cathodes go through the formation of a series of soluble higher-order polysulfide (PS) species (Li_2S_8 to Li_2S_4) during the discharge process and finally reduced to insoluble Li_2S_2 and Li_2S. While charging, Li_2S is first oxidized to various higher-order PSs and lastly to elemental sulfur. The polysulfide dissolution in the electrolyte results in the shuttling effect and consumption of sulfur and thereby ends up with rapid capacity fade and low Coulombic efficiency. Additionally, elemental sulfur which has a density of 2.03 g cm^{-3}, undergoes a volume expansion of approximately 80 % (density of Li_2S is 1.66 g cm^{-3}) during the electrochemical reaction as reported earlier.[3] Due to the volume changes the sulfur particles gets pulverized and this will eventually result in reduced capacity of Li–S batteries. Therefore, a balanced design of electrode structure is crucial to address these challenges.

Generally, the electronic conductivity of elemental sulfur can be enhanced by encapsulating sulfur in carbonaceous materials such as MWCNT or graphene or conducting polymeric materials.[7] Unfortunately, the conjugate non-polar carbon planes have limited sites to anchor the polar species [Li_2S_n] and offer only weak interactions. These weak interactions can at any time result in irremediable detachment of LiPSs from the cathode surface resulting in poor cycling performance. Further to address this issue anchoring of chemically binding sites for the PS intermediates with the introduction of polar sites onto the carbon planes has been widely explored.[8]

The integration of solid additives in the sulfur cathode has been recognized as an efficient way in trapping of polysulfides. Several efforts have also been made to restrain the polysulfides within the composite sulfur cathode by the introduction of

[a] D. E. Mathew, Prof. A. M. Stephan
CSIR- Central Electrochemical Research Institute,
Karaikudi 630 003, India
Tel.: +91 4565 241426
Fax: +91 4565 27779
E-mail: amstephan@cecri.res.in
[b] D. E. Mathew
Academy of Scientific and Innovative Research (AcSIR),
Ghaziabad 201002, India
[c] Dr. G. J. Rani
Fatima College (Autonomous),
Madurai 625 017, India
[d] D. P. Jenis
Sri Sivasubramaniya Nadar College of Engineering,
Kalavakkam, 603 110, India
[e] Prof. S. Thomas
Mahatma Gandhi University,
Kottayam, 686560, India

Supporting information for this article is available on the WWW under https://doi.org/10.1002/slct.202101479

inorganic materials such as $NiFe_2O_4$[7] and $MgAl_2O_4$,[9] owing to their strong electrostatic interaction of polysulfides. Very recently we have reported the cycling performance of Li S cell in which Fe_3O_4-seated rGO was incorporated as a solid additive in the sulfur cathode in order to improve the conductivity of sulfur and to confine polysulfide from shuttling.[10] Metal – organic frameworks have also been explored.[11–15] The specific chemical affinity of metal-based nanostructured materials to lithium polysulfides (LiPSs) effectively adsorb or even bind PS intermediates within the cathode scaffold. These 'chemisorptive' sulfur host materials improve the LiPS adsorption and thereby enhances the rate capability and active material utilization and cycling performance. Generally, the incorporation of a small dosage of additives increases the efficiency of Li–S batteries without increasing the cost compared with other methods. The addition of metal oxides in the composite sulfur cathode can improve the cycle life of Li–S batteries by modifying the morphology of the cathode effectively to promote electrochemical performance.

In the present work, nanostructured reduced graphene oxide attached with $MnFe_2O_4$ nanoparticles (rGO-$MnFe_2O_4$) was synthesized by a facile solvothermal process and successfully incorporated in a sulfur cathode as an additive. The integration of rGO-$MnFe_2O_4$ is expected to be favorable in two aspects; the added- rGO ensures improving the electrical conductivity while the nanostructured added- $MnFe_2O_4$ can effectively reduce the self-discharge and exhibited superior electrochemical performance. To analyze the role of $MnFe_2O_4$ the rGO/sulfur composite was also prepared and its cycling performance was analysed separately and the results are discussed.

Results and Discussion

Figure SI 1(a–f) (supporting information) shows the XRD patterns of $MnFe_2O_4$, graphene oxide, rGO, $MnFe_2O_4$- rGO, elemental sulfur and $MnFe_2O_4$- rGO- elemental sulfur composite respectively. The characteristic diffraction patterns found at $2\theta \approx 18.5$, 30.2, 35.6, 43.3, 53.8, 57.16, and 62.7 °, represents the (111), (220), (311), (400), (422), (511) and (440) reflection planes, respectively, (Figure SI 1a) were well matched with the standard powder diffraction pattern for the bulk cubic spinel-structured $MnFe_2O_4$ (JCPDS File no 74-2403).[16] The appearance of peak at $2\theta \approx 10.27°$ corresponds to (001) reflection plane arises from graphene oxide (Figure SI 1b) which further indicates complete oxidation of graphite.[17,18] The presence of $2\theta \approx 26.6°$ confirms the formation of rGO from graphene oxide (Figure SI 1c).[19] All the $MnFe_2O_4$ diffraction peaks were well preserved in rGO-$MnFe_2O_4$ composite (Figure SI 1d).[20] The non-existence of reflection plane corresponding to rGO at 26.6° indicated the removal of oxygen labile group from graphene sheets during the formation of rGO-$MnFe_2O_4$.[21,22]

The X-ray powder diffraction patterns of elemental sulfur are depicted in Figure SI 1e. The diffraction peaks of elemental sulfur are also seen unaltered in Figure SI 1f even after impregnation in the rGO-$MnFe_2O_4$ matrix. It is apparent from the Figure that the rGO- $MnFe_2O_4$ -sulfur ternary composite has peaks corresponding to $MnFe_2O_4$ with a comparatively reduced peak intensity to that of as synthesized $MnFe_2O_4$. The disappearance of characteristic Fddd orthorhombic crystal structure of elemental sulfur in ternary composite cathode in the XRD patterns is attributed to trapping of elemental sulfur into the internal layered structure of rGO. Further disappearance of new peaks in the composite sulfur cathode confirms that no chemical reaction has taken place between the composite components upon heat treatment.

The independent, yet distinctively uniform and precise spherical structures of $MnFe_2O_4$ particles with 370 nm average particle size were revealed through SEM (Figure SI 2 (a and b) and TEM images (Figure SI 2c). A close examination of the spherical structures of $MnFe_2O_4$ exposed that every individual sphere was composed of tiny particles of average size 10 nm aligned together as building blocks in a systematic manner to produce a well-defined spherical structure as displayed in Figure SI 2(d). The solvo-thermal method with modified reaction using $FeCl_3$ and $MnCl_2$ as precursors and $C_2H_3NaO_2$ as a base was used for the typical synthesis of $MnFe_3O_4$ spherical structures. In the synthesis of $MnFe_2O_4$ nanostructures, ethylene glycol ($C_2H_6O_2$) governed substantial role both as a reducing agent and as a solvent for the preparation. The alkaline surrounding developed by the $C_2H_3NaO_2$ induced the precipitation of Mn^{2+} and Fe^{3+} ions in the presence of ethylene glycol which respectively assisted in the formation of manganese(II) hydroxide and Iron(III) hydroxide that after the dehydration process were transposed to $MnFe_2O_4$ nanocrystals.[18] The high temperature developed during the reaction initiated the hydrolysis reaction which resulted in the formation of tiny $MnFe_2O_4$ primary particles, that clustered together to build bigger spheres. From TEM images rGO-$MnFe_2O_4$ composite, it is clear that $MnFe_2O_4$ particles were homogeneously dispersed over the crinkled, ultra-thin, undulating sheets of rGO.[23] The even distribution of $MnFe_2O_4$ nanoparticles over the rGO surface was aided through the electrostatic interaction between the negative charges on the rGO sheets and the positively charged metal ions (Mn^{2+}/Fe^{2+}) along with its concomitant reduction process. $MnFe_2O_4$ nanoparticles anchored over the rGO sheets exhibited ordered lattice fringes as shown in Figure 1 and the related SAED pattern showed the polycrystalline structure of $MnFe_2O_4$ nanomaterials.[24]

Figure SI 3(a–e) shows the Raman spectra of $MnFe_2O_4$, graphene oxide (GO), rGO, elemental sulfur and rGO-$MnFe_2O_4$-elemental sulfur composites respectively. The active Raman bands associated with the spinel ferrites is evidently visible in $MnFe_2O_4$ nanostructures ($A_{1g} + E_g + 3\ T_{2g}$). The T_{2g} (1) and E_g modes were respectively observed as bands at 210 and 270 cm^{-1}. The local lattice vibration of Fe^{3+} and O^{2-} found in the octahedral (Oh) sites of spinel structure has appeared as T_{2g} (2) mode from the band at 481 cm^{-1}. The T_{2g} (3) mode at 583 cm^{-1} evidently represent the stretching vibrations of Fe^{3+} and O^{2-} in the tetrahedral sites. The symmetric stretching mode of Fe–O at 673 cm^{-1} was weakened by the replacement of few Fe^{2+} ions in Fe_3O_4 by the Mn^{2+} ions to form $MnFe_2O_4$ nanostructures.[25] The two intense bands at 1340 and 1605 cm^{-1} of GO were displayed through the Raman spectrum

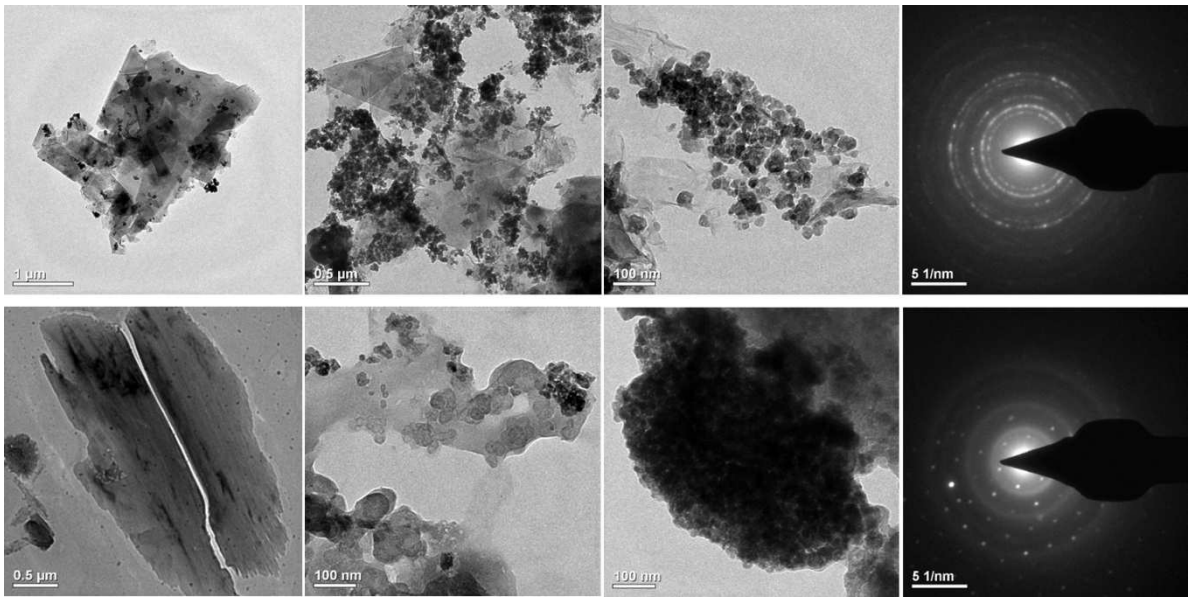

Figure 1. TEM images and corresponding SAED patterns of rGO-$MnFe_2O_4$-S cathode **Panel 1**: before cycling and **Panel 2**: after cycling.

(Figure SI 3b), denoting the D band originating from the sp^3 hybridized carbon atoms of disordered graphite and G band emerging from the sp^2 ordered graphite-like structures, respectively.[26] The rGO-$MnFe_2O_4$ composite maintained all the modes consistent to $MnFe_2O_4$ nanostructures with reduced intensities and considerable carbonaceous modes (Figure SI 3c). The I_D/I_G ratio of GO sheets was 0.89 and was increased to 1.12 for the rGO-$MnFe_2O_4$ composite, agreeing the presence of intensified structural defects and disorders.[27]

The content of sulfur in rGO-$MnFe_2O_4$- sulfur composite was obtained from thermogravimetric analysis in N_2 atmosphere as displayed in Figure SI 4 and the sulfur content was measured ~80%. The electrochemical performance of Li–S cells of rGO–S and rGO-$MnFe_2O_4$-S electrodes was then carried out by cyclic voltammetry and is displayed in Figure 2 a & b. It is quite obvious from Figures 2a and b that the voltammograms displayed two oxidation and reduction peaks regardless of added $MnFe_2O_4$. The reduction peaks appeared at 2.36 and 1.93 V denote the electrochemical reduction of sulfur into higher-order lithium polysulfides Li_2S_n ($n = 4 \leq 8$) and later these polysulfides are further reduced to insoluble lower-order polysulfides (Li_2S_2 and Li_2S).[28] During the charging process, the peaks observed at 2.36 and 2.45 V are ascribed to oxidation of insoluble polysulfides to higher-order lithium sulfides and further to sulfur. It is noteworthy that unlike the cell with rGO cathode, there was no discernible shift observed in the voltammogram peaks in the succeeding cycles showing there was no polarization effect in the Li–S cell.[29]

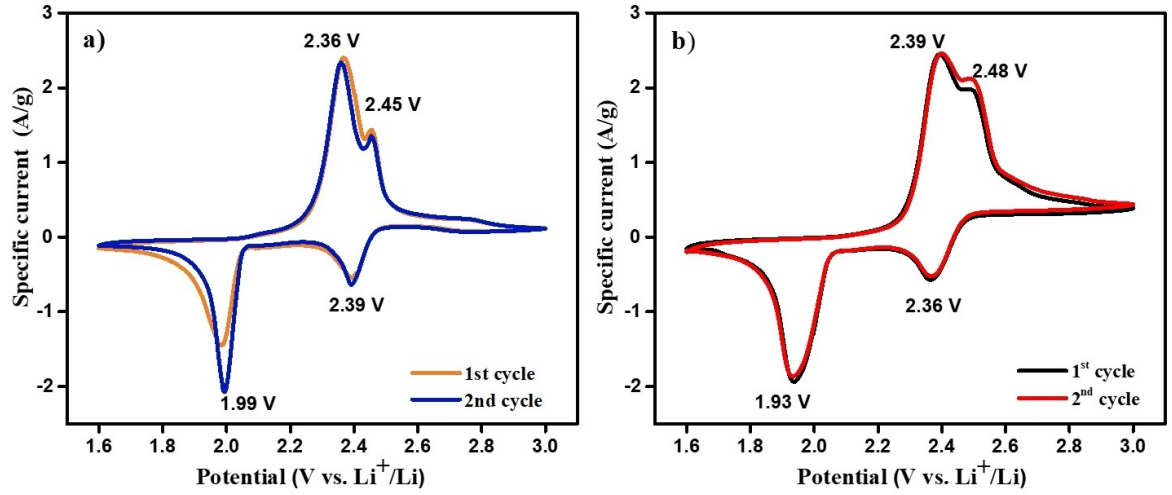

Figure 2. Cyclic voltammogram profiles of Li- S cell a) with rGO-sulfur cathode and b) rGO-$MnFe_2O_4$-sulfur composite cathode at a scan rate of 0.1 mVs^{-1}.

[7] Q. Fan, W. Liu, Z. Weng, Y. Sun, H. Wang, *J. Am. Chem. Soc.* **2015**, *137*, 12946.
[8] X. Liu, J. Q. Huang, Q. Zhang, L. Mai, *Adv. Mater.* **2017**, *29*, 1601759.
[9] M. Raja, K. Bicy, S. Suriyakumar, N. Angulakshmi, S. Thomas, A. M. Stephan, *Ionics* **2018**, *24*, 3451.
[10] S. Suriyakumar, G. J. Rani, A. M. Stephan, *Ionics* **2020**, *26*, 2201.
[11] H. Park, D. J. Siegel, *Chem. Mater.* **2017**, *29*, 4932.
[12] Z. Wang, B. Wang, Y. Yang, Y. Cui, Z. Wang, B. Chen, G. Qian, *ACS Appl. Mater. Interfaces* **2015**, *7*, 20999.
[13] S. Bai, K. Zhu, S. Wu, Y. Wang, J. Yi, M. Ishida, H. Zhou, *J. Mater. Chem. A* **2016**, *4*, 16812.
[14] S. Suriyakumar, M. Kanagaraj, M. Kathiresan, N. Angulakshmi, S. Thomas, A. M. Stephan, *Electrochim. Acta* **2018**, *265*, 151.
[15] S. Suriyakumar, A. M. Stephan, N. Angulakshmi, M. H. Hassan, M. H. Alkordi, *J. Mater. Chem. A* **2018**, *6*, 14623.
[16] G. H. Ren, Z. S. Yu, *Solid State Phenom.* **2012**, *181–182*, 393.
[17] J. G. Kim, J. wook Seo, J. Cheon, Y. J. Kim, *Bull. Korean Chem. Soc.* **2009**, *30*, 183.
[18] B. Antic, A. Kremenovic, N. Jovic, M. B. Pavlovic, C. Jovalekic, A. S. Nikolic, G. F. Goya, C. Weidenthaler, *J. Appl. Phys.* **2012**, *111*, 074309.
[19] G. J. Rani, K. J. Babu, G. G. kumar, M. A. J. Rajan, *J. Alloys Compd.* **2016**, *688*, 500.
[20] G. Gnana kumar, Z. Awan, K. Suk Nahm, J. Stanley Xavier, *Biosens. Bioelectron.* **2014**, *53*, 528.
[21] M. Vinothkannan, C. Karthikeyan, G. Gnana Kumar, A. R. Kim, D. J. Yoo, *Spectrochim. Acta Part A* **2015**, *136*, 256.
[22] G. P. J. Rani, J. Saravanan, S. Sheet, M. A. J. Rajan, Y. S. Lee, A. Balasubramani, G. G. kumar, *Electrocatalysis* **2018**, *9*, 102.
[23] C. L. Warner, W. Chouyyok, K. E. Mackie, D. Neiner, L. V. Saraf, T. C. Droubay, M. G. Warner, R. S. Addleman, *Langmuir* **2012**, *28*, 3931.
[24] X. Peng, J. Qu, S. Tian, Y. Ding, X. Hai, B. Jiang, M. Wu, J. Qiu, *RSC Adv.* **2016**, *6*, 104549.
[25] M. Y. Rafique, L. Q. Pan, Q. U. A. Javed, M. Z. Iqbal, H. M. Qiu, M. H. Farooq, Z. G. Guo, M. Tanveer, *Chinese Phys. B* **2013**, *22*, 107101.
[26] P. Song, X. Zhang, M. Sun, X. Cui, Y. Lin, *RSC Adv.* **2012**, *2*, 1168.
[27] I. Kotutha, E. Swatsitang, W. Meewassana, S. Maensiri, *Jpn. J. Appl. Phys.* **2015**, *54*, 06FH10.
[28] Z. W. Seh, Y. Sun, Q. Zhang, Y. Cui, *Chem. Soc. Rev.* **2016**, *45*, 5605.
[29] D. W. Wang, Q. Zeng, G. Zhou, L. Yin, F. Li, H. M. Cheng, I. R. Gentle, G. Q. M. Lu, *J. Mater. Chem. A* **2013**, *1*, 9382.
[30] F. Zhou, Z. Li, X. Luo, T. Wu, B. Jiang, L. L. Lu, H. Bin Yao, M. Antonietti, S. H. Yu, *Nano Lett.* **2018**, *18*, 1035.
[31] Z. Wang, Y. Dong, H. Li, Z. Zhao, H. Bin Wu, C. Hao, S. Liu, J. Qiu, X. W. D. Lou, *Nat. Commun.* **2014**, *5*, 5002.
[32] Q. Pang, J. Tang, H. Huang, X. Liang, C. Hart, K. C. Tam, L. F. Nazar, *Adv. Mater.* **2015**, *27*, 6021.
[33] Y. Zhang, Y. Zhao, A. Yermukhambetova, Z. Bakenov, P. Chen, *J. Mater. Chem. A* **2013**, *1*, 295.
[34] M. Helen, M. A. Reddy, T. Diemant, U. Golla-Schindler, R. J. Behm, U. Kaiser, M. Fichtner, *Sci. Rep.* **2015**, *5*, 12146.
[35] S. Drvarič Talian, G. Kapun, J. Moškon, A. Vizintin, A. Randon-Vitanova, R. Dominko, M. Gaberšček, *Chem. Mater.* **2019**, *31*, 9012.
[36] S. Drvarič Talian, J. Moškon, R. Dominko, M. Gaberšček, *ACS Appl. Mater. Interfaces* **2017**, *9*, 29760.
[37] M. Adamič, S. D. Talian, A. R. Sinigoj, I. Humar, J. Moškon, M. Gaberšček, *J. Electrochem. Soc.* **2019**, *166*, A5045.
[38] A. Ganesan, A. Varzi, S. Passerini, M. M. Shaijumon, *Electrochim. Acta* **2016**, *214*, 129.
[39] C. Barchasz, J. C. Leprêtre, F. Alloin, S. Patoux, *J. Power Sources* **2012**, *199*, 322.
[40] Z. Deng, Z. Zhang, Y. Lai, J. Liu, J. Li, Y. Liu, *J. Electrochem. Soc.* **2013**, *160*, A553.

Submitted: April 23, 2021
Accepted: July 27, 2021